Solution X-ray Scattering Reveals a Novel Structure of Calmodulin Complexed with a Binding Domain Peptide from the HIV-1 Matrix Protein p17[†]

Yoshinobu Izumi,*[,‡] Hiroki Watanabe,[‡] Noriko Watanabe,[‡] Aki Aoyama,[‡] Yuji Jinbo,[‡] and Nobuhiro Hayashi[§]

Graduate Program of Human Sensing and Functional Sensor Engineering, Yamagata University, 4-3-16, Jo-nan, Yonezawa, Yamagata 992-8510, Japan, and Institute for Comprehensive Medical Science, Fujita Health University, Toyoake, Aichi 470-1192, Japan

Received December 10, 2007; Revised Manuscript Received April 27, 2008

ABSTRACT: The solution structures of complexes between calcium-saturated calmodulin (Ca^{2+}/CaM) and a CaM-binding domain of the HIV-1 matrix protein p17 have been determined by small-angle X-ray scattering with use of synchrotron radiation as an intense and stable X-ray source. We used three synthetic peptides of residues 11−28, 26−47, and 11−47 of p17 to demonstrate the diversity of CaM-binding conformation. Ca^{2+}/CaM complexed with residues 11−28 of p17 adopts a dumbbell-like structure at a molar ratio of 1:2, suggesting that the two peptides bind each lobe of CaM, respectively. Ca^{2+}/CaM complexed with residues 26−47 of p17 at a molar ratio of 1:1 adopts a globular structure similar to the NMR structure of Ca^{2+}/CaM bound to M13, which adopted a compact globular structure. In contrast to these complexes, Ca^{2+}/CaM binds directly with both CaM-binding sites of residues 11−47 of p17 at a molar ratio of 1:1, which induces a novel structure different from known structures previously reported between Ca^{2+}/CaM and peptide. A tertiary structural model of the novel structure was constructed using the biopolymer module of Insight II 2000 on the basis of the scattering data. The two domains of CaM remain essentially unchanged upon complexation. The hinge motions, however, occur in a highly flexible linker of CaM, in which the electrostatic residues 74Arg, 78Asp, and 82Glu interact with N-terminal electrostatic residues of the peptide (residues 12Glu, 15Arg, and 18Lys). The acidic residues in the N-terminal domain of CaM interact with basic residues in a central part of the peptide, thereby enabling the central part to change the conformations, while an acidic residue in the C-terminal domain interacts with two basic residues in the two helical sites of the peptide. The overall structure of the complex adopts an extended structure with the radius of gyration of 20.5 Å and the interdomain distance of 34.2 Å. Thus, the complex is principally stabilized by electrostatic interactions. The hydrophobic patches of Ca^{2+}/CaM are not responsible for the binding with the hydrophobic residues in the peptide, suggesting that CaM plays a role to sequester the myristic acid moiety of p17.

Calmodulin (CaM)[1] is a ubiquitous Ca^{2+}-binding protein of 148 residues that regulates a variety of physiological processes in a Ca^{2+}-dependent manner (*1*). The regulation is achieved through the interaction of Ca^{2+}-saturated CaM (Ca^{2+}/CaM) with a large number of target proteins that are functionally and structurally diverse (*2, 3*). The structure of Ca^{2+}/CaM adopts an extended structure (*4*) in which the two domains are connected by a highly flexible linker (*5–7*), whereas the structures of Ca^{2+}/CaM complexed with a peptide from target proteins adopt a compact globular structure caused by the bending of the flexible linker (*8, 9*). Recently, however, an extended but not collapsed structure of CaM found in the complexes with a model peptide and the crystal of CaM-regulated adenylate cyclase suggests that CaM should regulate target proteins with versatile ways (*10*).

It has been reported that CaM binds the structural proteins of human immunodeficiency virus type 1 (HIV-1), Gag and the matrix protein (p17), in a Ca^{2+}-dependent manner and that there are two nearly contiguous CaM-binding sites contained in residues 11−46 of p17 (*11*). The p17 of HIV-1 is produced by proteolytic processing of the precursor Gag polyprotein (*12, 13*). The mature p17 performs important functions in early stages of the viral cycle. Two major functions for p17 have been clearly established. (i) p17 is critical to the targeting of the Gag precursor to the plasma membrane. Mutation of the N-terminal Gly abolishes virus assembly in most systems (*14–16*). Mutation of a highly basic domain near the N terminus of p17 (residues 17−31) disrupts proper Gag targeting and virus assembly (*17–19*). (ii) p17 is required for efficient incorporation of the envelope glycoproteins into virions. Deletions and multiple amino acid substitutions throughout the majority of p17 impair the envelope incorporation (*20, 21*), and single amino acid substitutions near the amino terminus of p17 (e.g., at residues 10, 12, 30, and 34) abolish or significantly reduce the envelope incorporation (*22–24*). Thus, the mutation studies

[†] The SAXS measurements were performed with approval of the Photon Factory Committee, KEK, Tsukuba, Japan (Proposal Nos. 01G365, 03G329, 05G296, and 07G545).

* To whom correspondence should be addressed. Tel: 81-238-26-3183. Fax: 81-238-26-3177. E-mail: yizumi@yz.yamagata-u.ac.jp.

[‡] Yamagata University.

[§] Fujita Health University.

[1] Abbreviations: CaM, calmodulin; SAXS, small-angle X-ray scattering; A, Ala; C, Cys; D, Asp; E, Glu; F, Phe; G, Gly; H, His; I, Ile; K, Lys; L, Leu; M, Met; N, Asn; P, Pro; Q, Gln; R, Arg; S, Ser; T, Thr; V, Val; W, Trp; Y, Tyr.

10.1021/bi702416b CCC: $40.75
Published on Web 06/14/2008

Table 1: Primary Sequences of Three Peptides of p17 Synthesized in This Work

peptide name	primary sequence	AA[a]
p17(11−28)	GELDRWEKIRLRPGGKKK	18
p17(26−47)	KKKYKLKHIVWASRELERFAVN	22
p17(11−47)	GELDRWEKIRLRPGGKKKY KLKHIVWASRELERFAVN	37

[a] AA represents the number of amino acid residues; underlined sequences denote helices, which are referred from the Protein Data Bank code of p17 (1tam).

produce results consistent with the possibilities that CaM might be involved in the targeting process and also in modulation of myristoylation effects. However, little is known about the role of CaM binding to Gag. In order to reveal the role, the structural and modeling studies on the complexes are crucial.

In this report, we have investigated the solution structure of the complexes by small-angle X-ray scattering (SAXS) with use of synchrotron radiation as an intense and stable X-ray source, which is a useful method to detect direct interaction between CaM and target peptides through measurable structural changes of CaM. We used three synthetic peptides of residues 11−28, 26−47, and 11−47 from p17 as a target for CaM to demonstrate the diversity of CaM-binding conformation. The main SAXS results indicate that Ca^{2+}/CaM binds directly with two CaM binding sites of p17(11−47) and induces a novel structure different from that previously reported between Ca^{2+}/CaM and peptides. A tertiary structural modeling of the complex predicts that the overall structure of the complex of Ca^{2+}/CaM and p17(11−47) adopts an extended structure and is principally stabilized by electrostatic interactions, suggesting that the hydrophobic patches of Ca^{2+}/CaM interact with the myristic acid moiety of p17, if the present model mimics the corresponding part of a Ca^{2+}/CaM/p17 complex.

MATERIALS AND METHODS

Materials. The recombinant CaM based on the sequence of rat CaM was expressed as described in ref *25*. CaM fraction was obtained as described in ref *26*. The peptides were synthesized and purified as described in ref *27*. Table 1 summarizes the primary sequences of three synthetic peptides of p17. These peptides correspond to residues 11−28, 26−47, and 11−47 of p17, which are denoted hereafter by p17(11−28), p17(26−47), and p17(11−47), respectively.

SR-SAXS Measurements. The basic medium used for the SAXS measurements was 50 mM Tris-HCl, pH 7.6, and 120 mM NaCl. A complex of Ca^{2+}/CaM with each peptide of p17 was prepared by mixing the protein with both a 4.4-fold molar excess of Ca^{2+} and 1.1 or 2.2 mol of the peptide. The molar ratios of the peptide were prepared according to a previous intrinsic tryptophan fluorometry (*11*). The protein concentrations for both Ca^{2+}/CaM/p17(11−28) and Ca^{2+}/CaM/p17(26−47) were 7.5, 10.0, 12.5, 15.0, 17.5, and 20.0 mg/mL, while those for Ca^{2+}/CaM/p17(11−47) were 5.0, 7.5, 10.0, 12.5, and 15.0 mg/mL. The concentrations of proteins were determined by the method described in ref *28*.

The SAXS profiles for all samples were acquired using the instrument for SAXS installed at BL-10C of Photon Factory, KEK, Tsukuba. The details of the optics and instruments are given elsewhere (*29*). An X-ray wavelength of 1.488 Å was selected. The samples were contained in a mica cell with a volume of 70 μL, and the temperature was kept at 25.0 ± 0.1 °C by circulating water through the cell holder. The reciprocal parameter, s, equal to $(2 \sin \theta)/\lambda$, was calibrated by the observation of a chicken collagen, where 2θ is the scattering angle and λ is the X-ray wavelength. Scattering data were collected for 300 s at various concentrations. Irradiation of all samples for periods up to 1800 s produced no change in the scattering profiles.

Scattering Data Analysis. Three methods of data analysis were used. The first method was that of Guinier and Fournet (*30*). The scattering intensity of $I(s,c)$ measured as a function of s at a finite protein concentration, c, is given by

$$I(s,c) = I(0,c) \exp\{-(4\pi^2/3)R_g(c)^2 s^2\} \quad (1)$$

Here $I(0,c)$ is the scattering intensity at $s = 0$ and $R_g(c)$ is the radius of gyration as a concentration c. In the dilute limit, $I(0,c)$ is given by

$$Kc/I(0,c) = 1/M + 2A_2 c + ... \quad (2)$$

where K is a constant, M is the molecular weight of the protein, and A_2 is the second virial coefficient. The K value was determined using a Ca^{2+}/CaM or Ca^{2+}/CaM/MLCK peptide complex as a standard sample. In the dilute limit, $R_g(c)$ is given by

$$R_g(c)^2 = {R_0}^2 - B_{if} c + ... \quad (3)$$

where R_0 is the radius of gyration at infinite dilution and B_{if} is the parameter of interparticle interference (*31*). B_{if} can be related to $A_2$for particles with spherical symmetry (*30*).[2] For particles without spherical symmetry, it contains another term different from that of A_2, because the square of the average of the structure factor is not equal to the average of the square of the structure factor any more. Therefore, B_{if} has been used as another interaction parameter different from A_2 (*31*). Using eqs 2 and 3, we evaluated the four parameters M, A_2, R_0, and B_{if}. For the analysis, the range of s^2 (Å^{-2}) for each complex was determined by using a Guinier condition of $(4\pi^2/3)R_g(c)^2 s^2 < 1$.

The second method was that of that of Kratky, which is defined by the plot of $s^2 I(s)$ versus s (the Kratky plot) (*32*). The Kratky plots provide the structural characteristics (e.g., molecular shape) of a chain polymer and a biopolymer. The Kratky plot from a mixture of states 1 and 2 was calculated by

$$s^2 I(s)_{mixture}/I(0)_{mixture} = s^2[p_1 I_1(s) + p_2 I_2(s)]/[p_1 I_1(0) + p_2 I_2(0)] \quad (4)$$

where p_1 and p_2 are the probability of states 1 and 2, respectively (*30*).

The third method was that of Svergun (*33*), in which GNOM and DAMMIN were used to evaluate the distance distribution function ($P(r)$) and the molecular shape for a complex, respectively.[3] For the analysis, all data to $s = 0.06$ Å^{-1} were used.

[2] Reference 30 is available via UMI Books on demand, UMI, a Bell & Howell Co., 300 North Zeeb Road, P.O. Box 1346, Ann Arbor, MI 48106-1346 (800-521-0600, 313-761-4700).

[3] GNOM and DAMMIN are available free of charge via the Internet at http://www.ill.fr/lss/data_treatment/SAS_analysis.html.

The error bars are usually denoted in the case where the experimental errors are larger than the symbols.

Tertiary Structural Prediction. A predicted tertiary structural model of the Ca^{2+}/CaM/p17(11−47) complex was constructed using the biopolymer module of Insight II 2000 (Accerlys). Sequential morphs of CaM were obtained from prediction of movement accompanying with conformational change between the Ca^{2+}/CaM/RS20 complex (ff0 form (PDB: 1cdl)) and Ca^{2+}/CaM (ff17 form (PDB: 1cll)) (*34*). Three conformations of CaM (ff11, ff13, and ff15) were finally selected and probed with reference of experimental data to their calculated R_g, the shape of the SAXS profile, and that of the Kratky plot. An initial conformation of p17 was extracted from the coordinate of Gag protein (PDB: 1tam) and was placed on an initial position using arrangement of M13 (the CaM-binding site of skeletal muscle myosin light chain kinase (skMLCK) (residues 577−602)) in the complex with CaM as reference (PDB: 2bbn). The geometry of the initial models was optimized using CVFF force field (*35*). Then, to search the most stable arrangement of p17 complexed with CaM, the systems were equilibrated through 5 ps of NVT-molecular dynamics at 298 K, in which only residues of p17 were allowed to move while conformations of CaM were fixed. The program Discover 3 module of Insight II 2000 (Accerlys) was used for energy minimization and the molecular dynamic calculations. Thus, each set of coordinates for three candidates was obtained, and the model best fitted to the SAXS data (ff15) was presented in the text.

Calculation of SAXS Profile of Known Tertiary Structures. To compute $I(s)$ for each candidate, the Debye's formula has been extended taking into account the solvent-inaccessible volume, as described in ref *36*, and normalized:

$$I(s)/I(0) = \{I_{a-a}(s) - 2I_{a-b}(s) + I_{b-b}(s)\}/\{I_{a-a}(0) - 2I_{a-b}(0) + I_{b-b}(0)\} \quad (5)$$

where

$$I_{a-b}(s) = \sum\sum f_m^{\,a} f_n^{\,b} \sin(2\pi s R_{mn})/(2\pi s R_{mn}) \quad (6)$$

$$I_{a-b}(0) = \sum\sum f_m^{\,a} f_n^{\,b} \quad (7)$$

Here, N is the number of discrete scattering elements, and the superscripts "a" and "b" refer to the protein molecule and the solvent, respectively. f_m and f_n are the number of electrons for the mth element and the nth element, respectively. R_{mn} is the distance between the elements m and n. The double summation encompasses all scattering elements in the assemblage. The normalized Kratky plot ($s^2 I_{a-b}(s)/I_{a-b}(0)$ versus s) was calculated from the corresponding normalized SAXS profile. The Vax Fortran program written originally in ref *36* was properly rewritten using Fortran 77, and all computations were performed on a Fujitsu PC (Windows XP) using Cygwin.

RESULTS

Guinier Region of the Scattering Profile. An example of Guinier plots (ln $I(s)$ versus s^2) for a complex of Ca^{2+}/CaM/p17 peptide over the concentration series is shown in Figure 1A−C. In all of the samples studied here, there is no evidence of any upward curvature at low s (*2*) values in the Guinier plots, which indicates that the data are free from

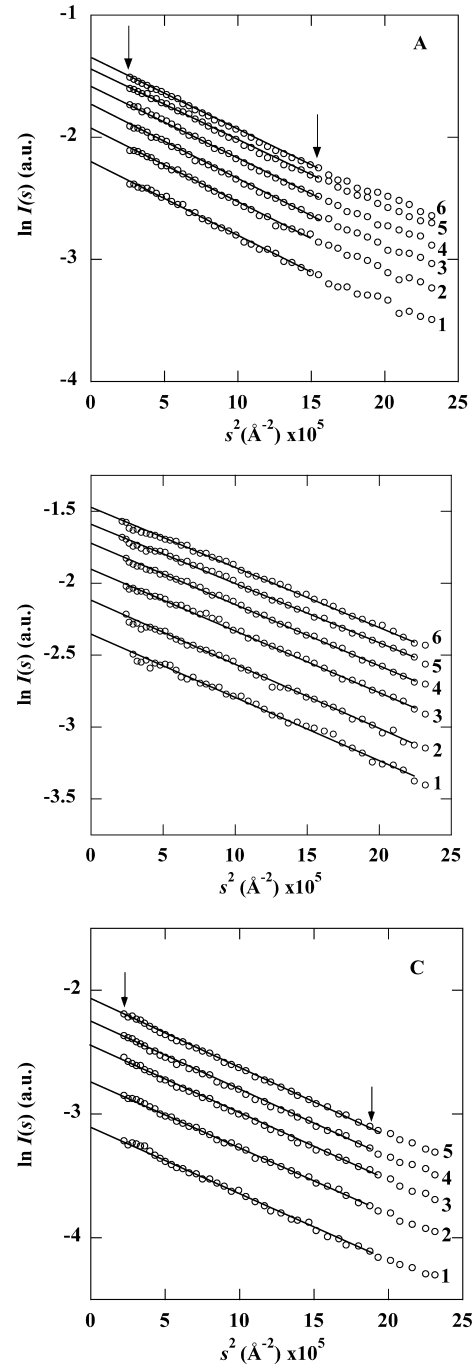

FIGURE 1: Guinier plots for a complex of Ca^{2+}/CaM/p17 peptide at a molar ratio of 1:1 at various protein concentrations. The straight lines were obtained with the data points between the arrows in the figure by the least-squares method. (A) CaM/p17(11−28) and (B) CaM/p17(26−47): (1) 7.5 mg/mL; (2) 10.0 mg/mL; (3) 12.5 mg/mL; (4) 15.0 mg/mL; (5) 17.5 mg/mL; (6) 20.0 mg/mL. (C) CaM/p17(11−47): (1) 5.0 mg/mL; (2) 7.5 mg/mL; (3) 10.0 mg/mL; (4) 12.5 mg/mL; (5) 15.0 mg/mL.

the aggregation of the samples. The values of $Kc/I(0,c)$, evaluated from the intercepts of the Guinier plots for all samples, are shown in Figure 2A as a function of protein concentration. The plots are linear over the entire concentration range, and the value of $[Kc/I(0,c)]_{c=0}$ extrapolated to infinite dilution for each complex has the inverse molecular weight appropriate for the soluble monomer.

The molecular weights M and the second virial coefficients A_2 were compiled in Table 2. The experimental values of M for all complexes almost agree well with the calculated values

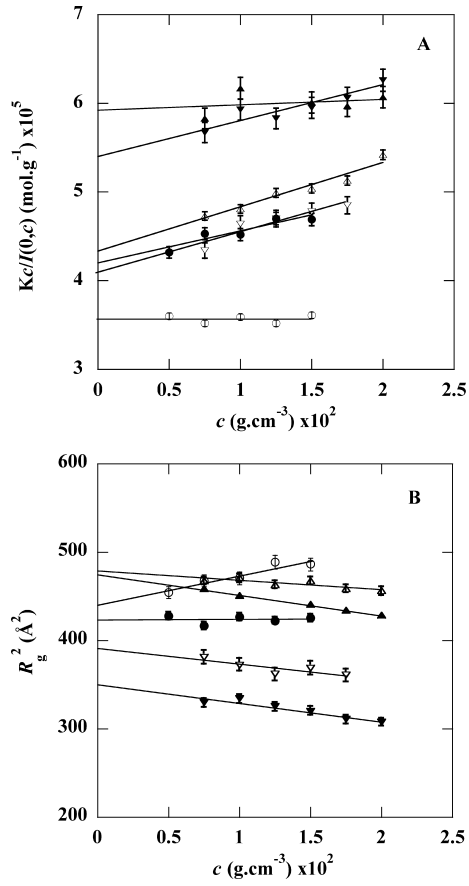

FIGURE 2: (A) Zimm plots for a complex of Ca^{2+}/CaM/p17 peptide. (B) The square of the radius of gyration, R_g^2, for a complex of Ca^{2+}/CaM/p17 peptide as a function of the protein concentration: (▲, △) Ca^{2+}/CaM/p17(11−28); (▼, ▽) Ca^{2+}/CaM/p17(26−47); (●, ○) Ca^{2+}/CaM/p17(11−47). Filled symbols denote a molar ratio of 1:1, while open symbols denote a molar ratio of 1:2.

denoted in parentheses within the experimental error of about 10%, except that for the complex of Ca^{2+}/CaM/p17(11−47) at a molar ratio of 1:1. The latter value obtained experimentally is 12% larger than the calculated value of monomer (M_1) and seems to be slightly over the experimental error. We believe this slight difference is not due to aggregations but experimental uncertainties. If this increment is due to aggregation, the molecular weight represents the weight average molecular weight (M_w). As no upturn was observed at the lowest s^2 region, as seen from Figure 1C, the size of aggregates is not so large, and probably the contribution from dimers (M_2) would be predominant. The molar fraction of dimers (x_2) was estimated to be 0.064, whose value is small compared with that of monomers ($x_1 = 0.936$), even if the solution could contain dimers. Here x_2 ($=1 - x_1$) was calculated by $M_w/M_1 = \{x_1M_1^2 + x_2M_2^2\}/\{x_1M_1^2 + x_2M_1M_2\} = 1.12$. In this point, a previous intrinsic tryptophan fluorometry (*11*) has showed that Ca^{2+}/CaM binds p17(11−25) with a 1:2 stoichiometry and a dissociation constant of approximately 10^{-9} M^2 and that it also binds p17(31−46) with a 1:1 stoichiometry and a dissociation constant of approximately 10^{-9} M. Therefore, it is reasonable to conclude that Ca^{2+}/CaM binds each peptide with the molar ratio described in Table 2.

Radii of gyration at infinite dilution were calculated from the slopes of the Guinier plots and are shown in Figure 2B. The linear increase with decreasing protein concentration was observed in the complexes for Ca^{2+}/CaM/p17(11−28) and Ca^{2+}/CaM/p17(26−47), while the linear decrease was observed in the Ca^{2+}/CaM/p17(11−47) complex at a molar ratio of 1:2, but no protein concentration dependence was observed in the Ca^{2+}/CaM/p17(11−47) complex at a molar ratio of 1:1. The slopes of these lines, which arise from interparticle interference effects, represent a virial coefficient (*30*). Table 2 also compiles the values of R_0 and B_{if}.

The R_0 value for the Ca^{2+}/CaM/p17(11−28) complex with 2 mol of p17(11−28) and without p17(11−28) is 21.8 ± 0.3 Å, a value typical of the dumbbell-shaped structure (*4, 5, 27, 37*). The R_0 value does not almost change by the binding of 2 mol of the peptide, suggesting that the molecular shape still adopts a dumbbell-shaped structure. However, the tendencies of A_2 and B_{if} are totally different: the value of A_2 of the complex with 2 mol of p17(11−28) and without p17(11−28) is smaller than that at a molar ratio of 1:2, while that of B_{if} is reversed each other.

The R_0 value for the Ca^{2+}/CaM/p17(26−47) complex is 18.7 ± 0.3 Å at a molar ratio of 1:1, whose value is close to a typical value of the globular structure (*38–40*), and it increases by 1.1 ± 0.3 Å by the binding of 2 mol of the peptide. However, their tendencies for the interactions almost do not change by the binding of 2 mol of the peptide.

The R_0 value for the Ca^{2+}/CaM/p17(11−47) complex is 20.5 ± 0.3 Å at a molar ratio of 1:1, and it increases by 0.5 Å by the binding of 2 mol of the peptide. If the R_0 value of 20.5 Å corresponds to a mixture, the R_0 value represents a z-averaged radius of gyration (R_z). The R_z value is given by $R_z^2 = \{p_1I_1(0)R_1^2 + p_2I_2(0)R_2^2\}/\{p_1I_1(0) + p_2I_2(0)\}$ (*30*). For a mixture of the Ca^{2+}/CaM/p17(11−28) complex with 2 mol of p17(11−28) and without p17(11−28) and the Ca^{2+}/CaM/p17(26−47) complex at a molar ratio of 1:1, the R_z value was estimated at 20.2 Å. As this value is close to the R_0 value (20.5 ± 0.3 Å) for the Ca^{2+}/CaM/p17(11−47) complex at a molar ratio of 1:1, the Ca^{2+}/CaM/p17(11−47) complex might be interpreted as the mixture. The interpretation is, however, evidently contrary to the results of the interaction parameters. That is, the value of A_2 for the Ca^{2+}/CaM/p17(11−47) complex at a molar ratio of 1:1 is positive, while the value of B_{if} for the same complex is almost zero. The values of A_2 and B_{if} for the Ca^{2+}/CaM/p17(11−28) complex are both positive. The corresponding values for the Ca^{2+}/CaM/p17(26−47) complex are also both positive. As a result, both A_2 and B_{if} for the predicted mixture would be expected to be positive, although the quantitative evaluation is quite complicated. Thus, their interactions for the Ca^{2+}/CaM/p17(11−47) at a molar ratio of 1:1 could not be interpreted as the mixture of above states would be expected to be, allowing them to conclude that the 1:1 binding of CaM to the peptide is induced by a specific interaction. In addition, the drastic decrease of the interaction parameters associated with the binding of 2 mol of peptide was observed, suggesting a decrease in the net charge of the complex.

Kratky Region of the Scattering Profile. Figure 3A shows the Kratky plot for the Ca^{2+}/CaM/p17(11−28) complex which is characterized by the presence of a broad peak near $s = 0.012-0.023$ Å^{-1}, indicating that the complex adopts a dumbbell-shaped structure, which is close to a dumbbell-like structure denoted by a green solid line for Ca^{2+}/CaM (*41*). The shape does not almost change by the binding of 2 mol of the peptide, which is consistent with the result of the

Table 2: Molecular Weight (M) and Second Virial Coefficient (A_2), Radius of Gyration at Infinite Dilution (R_0), and Parameter of Interparticle Interference (B_{if}) for a Complex of Ca^{2+}/CaM/p17 Peptide

CaM/p17 peptide (molar ratio)	$10^{-3}M$ (g/mol) (calcd value)[a]	10^4A_2 (mol·cm^3/g^2)	R_0 (Å)	$10^{13}B_{if}$ (cm^5/g)
CaM/p17(11−28) (1:0 + 1:2)	16.9 ± 1.5 (18.0)	0.3 ± 0.2	21.8 ± 0.3	2.3 ± 0.2
CaM/p17(11−28) (1:2)	23.1 ± 2.1 (21.2)	2.5 ± 0.2	21.9 ± 0.3	1.0 ± 0.1
CaM/p17(26−47) (1:1)	18.5 ± 1.7 (19.6)	1.9 ± 0.2	18.7 ± 0.3	2.1 ± 0.2
CaM/2p17(26−47) (1:2)	24.5 ± 2.2 (22.4)	2.3 ± 0.2	19.8 ± 0.3	1.8 ± 0.2
CaM/p17(11−47) (1:1)	24.0 ± 2.2 (21.4)	1.8 ± 0.2	20.5 ± 0.3	−0.1 ± 0.1
CaM/p17(11−47) (1:2)	28.1 ± 2.5 (25.9)	0.0 ± 0.1	21.0 ± 0.3	−3.5 ± 0.2

[a] M for a complex of CaM/p17 peptide was calculated.

radius of gyration. Figure 3B shows the Kratky plot for the Ca^{2+}/CaM/p17(26−47) complex which is characterized by the presence of a sharp peak near $s = 0.015$ Å^{-1}, indicating that the complex adopts a globular structure, as it is close to a compact globular structure denoted by a blue solid line for a Ca^{2+}/CaM/MLCK22 complex (*41, 42*). The globular structure somewhat expands by the binding of 2 mol of the peptide, as the corresponding peak in the Kratky plot evidently decreases by the binding of 2 mol of the peptide. In contrast to the results for these complexes, Figure 3C shows the Kratky plot for the Ca^{2+}/CaM/p17(11−47) complex, which is characterized by the presence of an asymmetric peak near $s = 0.014$ Å^{-1}, suggesting that the molecular states resemble neither the dumbbell-shaped structure for the Ca^{2+}/CaM (green line) nor the compact globular structure for the Ca^{2+}/CaM/MLCK22 complex (blue line). Moreover, the Kratky plot for a mixture of Ca^{2+}/CaM (green line) and the Ca^{2+}/CaM/p17(11−47) complex (open circles in Figure 3C) and that for a mixture of the Ca^{2+}/CaM/p17(11−28) complex (filled triangles in Figure 3A) and the Ca^{2+}/CaM/p17(26−47) complex (filled triangles in Figure 3B) have been calculated according to eq 4. The former is denoted by a red solid line and the latter by a red dotted line in Figure 3C, respectively, in which both plots were calculated at a molar ratio of 1:1. Thus, neither of these mixtures will reproduce the Kratky plot of the Ca^{2+}/CaM/p17(11−47) complex at a molar ratio of 1:1. On the other hand, the molecular weight and the radius of gyration have been calculated as 22.3×10^3 g/mol and 21.2 Å for the former and 18.8×10^3 g/mol and 20.2 Å for the latter, respectively. The corresponding experimental values for the Ca^{2+}/CaM/p17(11−47) complex at a molar ratio of 1:1 are $(24.0 \pm 2.2) \times 10^3$ g/mol and 20.5 ± 0.3 Å, respectively. Thus, every one of these mixtures does not satisfy the experimental results. Other possible mixtures have been tested, but none of these can reproduce the plot. Taken together, it is reasonable to suggest that the Ca^{2+}/CaM/p17(11−47) complex at a molar ratio of 1:1 adopts a novel structure. The structure somewhat expands by the binding of 2 mol of the peptide, as the corresponding peak in the Kratky plot evidently decreases by the binding of 2 mol of the peptide, suggesting that the Ca^{2+}/CaM/p17(11−47) complex at a molar ratio of 1:2 also adopts a novel structure.

Figure 4A shows a comparison among three $P(r)$ curves for the Ca^{2+}/CaM/p17(11−28) complex at a molar ratio of 1:2 (green curve), Ca^{2+}/CaM/p17(26−47) complex at a molar ratio of 1:1 (blue line), and Ca^{2+}/CaM/p17(11−47) complex at a molar ratio of 1:1 (red line), which were derived from the corresponding scattering curves by GNOM (*33*). The $P(r)$ curve of Ca^{2+}/CaM/p17(26−47) shows only one maximum, which is consistent with a globular structure. The maximum dimension of the complex is around 55.0 Å. In contrast, both complexes of Ca^{2+}/CaM/p17(11−28) and Ca^{2+}/CaM/p17(11−47) adopt an extended structure. The maximum $P(r)$ value, the shoulder, and the maximum dimension for the former fall near 20.4, 32.0, and 67.4 Å, respectively, while those for the latter fall near 21.5, 32.7, and 67.4 Å, respectively. Although these values are similar to each other, it should be noted that the overall shapes of the $P(r)$ curve differ obviously from each other. Figure 4B shows the molecular shapes corresponding to three complexes shown in Figure 4A, which were derived from the corresponding GNOM data by DAMMIN (*33*). It is easily seen that the Ca^{2+}/CaM/p17(26−47) complex is a globular structure, while both complexes of Ca^{2+}/CaM/p17(11−28) and Ca^{2+}/CaM/p17(11−47) are different types of extended structures. The Ca^{2+}/CaM/p17(11−28) complex adopts a straight dumbbell-shaped structure, while the Ca^{2+}/CaM/p17(11−47) complex adopts a bent one.

DISCUSSION

This work verifies the diversity of CaM-binding conformation. Although there is no canonical CaM-binding motif in the sequence of p17(11−28), Ca^{2+}/CaM binds the peptide. As the deletion of 16Trp17Glu18Lys reduces gp160 incorporation (*19*), it has been suggested that these three residues are involved in the CaM binding. The straight dumbbell-shaped structure for the Ca^{2+}/CaM/p17(11−28) complex could be originated from that one peptide binds one domain of Ca^{2+}/CaM, while the other does another domain. On the other hand, the Ca^{2+}/CaM/p17(26−47) complex at a molar ratio of 1:1 adopts a globular structure, and the X-ray crystallographic structure of p17 shows the secondary structural assignment of this region to be a helix. Although the recognition motif has not been confirmed, it is suggested that Ca^{2+}/CaM recognizes a motif of residues 31Leu, 35Val, and 44Phe with the exception of 38Ser at the eighth position, which fits a 1-5-8-14 motif of hydrophobic residues shown in the NMR structure of a M13 bound to Ca^{2+}/CaM (*8*). The exception at the eighth position could explain a slightly larger value of R_0 for the complex, because this residue is required for binding both domains of CaM (*8*). The Ca^{2+}/CaM/p17(26−47) complex at a molar ratio of 1:2 adopts a somewhat relaxed globular structure, suggesting that the second p17(26−47) also participates in the interaction between two domains of CaM. These structural studies suggest that the flexibility of the central linker and the two hydrophobic patches in Ca^{2+}/CaM play an important role in target recognition.

In contrast to these complexes, Ca^{2+}/CaM binds directly with both CaM-binding sites of residues 11−47 of p17 at a molar ratio of 1:1, which induces a novel structure different from known structures previously reported between Ca^{2+}/

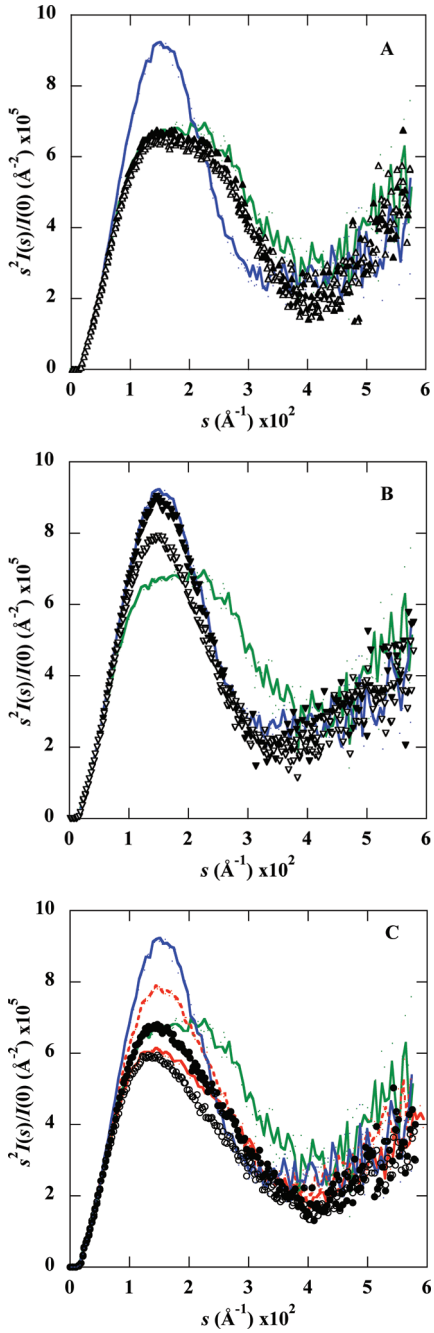

FIGURE 3: Kratky plots for a complex of Ca^{2+}/CaM/p17 peptide at the protein concentration of 15.0 mg/mL: (A) Ca^{2+}/CaM/p17(11−28); (B) Ca^{2+}/CaM/p17(26−47); (C) Ca^{2+}/CaM/p17(11−47). Filled symbols denote a molar ratio of 1:1, while open symbols denote a molar ratio of 1:2. The green and blue lines correspond to the Kratky plots for Ca^{2+}/CaM with a dumbbell-like structure and Ca^{2+}/CaM/MLCK22 with a compact globular structure, respectively (*41, 42*); also see Materials and Methods. These standard samples have been measured in parallel with the samples investigated in this work. The red solid and dotted lines in panel C denote a combined curve of the Kratky plot of Ca^{2+}/CaM/p17(11−47) (open circles in panel C) and that of Ca^{2+}/CaM and a combined curve of the Kratky plot of Ca^{2+}/CaM/p17(11−28) (filled triangles in panel A) and that of Ca^{2+}/CaM/p17(26−47) (filled triangles in panel B), respectively. Here, each combined curve was calculated according to eq 4, in which $p_1 = p_2 = 0.5$.

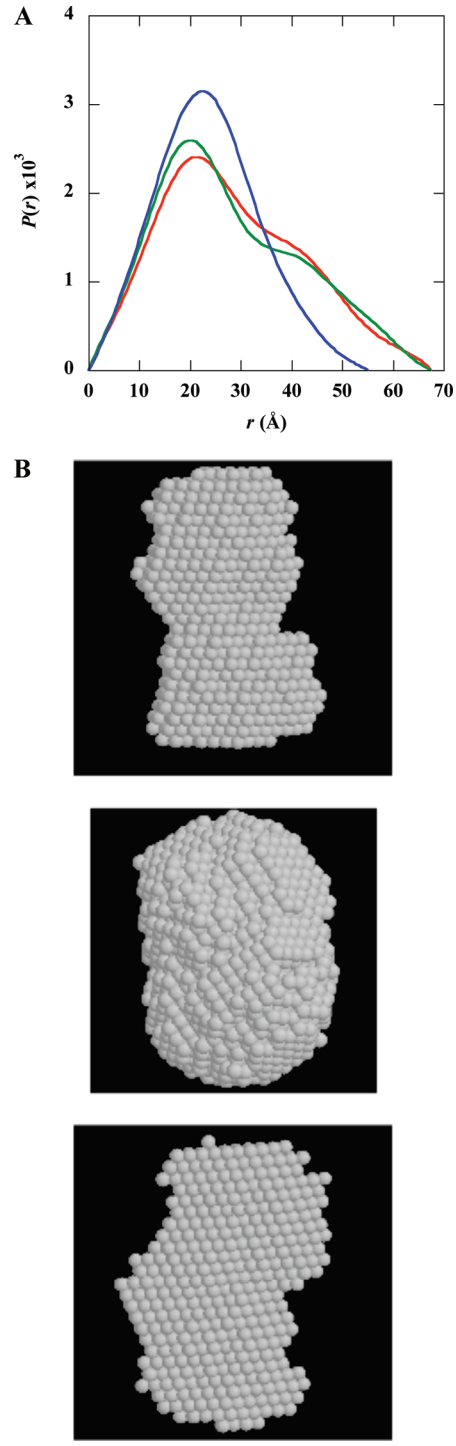

FIGURE 4: (A) Comparison of $P(r)$ curves for three complexes: Ca^{2+}/CaM/p17(11−28) complex at a molar ratio of 1:2 (green curve), Ca^{2+}/CaM/p17(26−47) complex at a molar ratio of 1:1 (blue line), and Ca^{2+}/CaM/p17(11−47) complex at a molar ratio of 1:1 (red line), which were calculated by GNOM (*33*). (B) The molecular shapes corresponding to the three complexes shown in (A), which were obtained by DAMMIN (*33*). The top corresponds to the Ca^{2+}/CaM/p17(11−28) complex, the middle to the Ca^{2+}/CaM/p17(26−47) complex, and the bottom to the Ca^{2+}/CaM/p17(11−47) complex, in which the corresponding maximum dimensions are around 67.4, 55.0, and 67.4 Å, respectively.

CaM and peptide. Therefore, we tried more detailed tertiary structural prediction from the SAXS profile. Taking into account that the dissociation constants of the two peptides for Ca^{2+}/CaM are almost the same order (*11*), the most straightforward interpretation for the result of the Ca^{2+}/CaM/p17(11−47) complex is that the two domains of Ca^{2+}/CaM interact directly with residues 11−25 and 31−46 of p17(11−47). As the overall structure of p17(11−47) has not been known, the total structure of p17 (PDB: 1tam) evaluated

by NMR was referred. It shows that residues 11−18 are a helix, as are residues 30−45 (*43, 44*). With regard to the arrangement of the two helices, the NMR structure was selected as a reasonable arrangement. In the NMR structure selected, there are two groups of bulky hydrophobic residues: the first consists of 13Leu, 16Trp, 31Leu, and 35Val, while the second consists of 36Trp, 41Ile, and 44Phe. It is noted that 13Leu and 16Trp are located close to 31Leu and 35Val, suggesting that these residues might interact with one domain of CaM. On the other hand, it is suggested that 36Trp, 41Ile, and 44Phe might interact with the other domain. Thus, it is suggested that the direct binding of CaM with these two CaM-binding sites of p17(11−47) induces a novel dumbbell-shaped structure. As these hydrophobic residues are located inside p17, the CaM-binding might request a drastic conformational change of p17. However, the NMR structure of p17 is equivalent with that of the crystal structure, suggesting that the whole structure of p17 is still preserved upon binding of CaM (*43, 44*). Therefore, it has been required to estimate directly the residue pairs interacting between CaM and p17(11−47) based on a tertiary structural model predicted by the SAXS data.

The tertiary structural prediction for Ca^{2+}/CaM complexed with the CaM-binding domain of p17(11−47) has been performed, as described in the Materials and Methods. There are many combinations matched to CaM in morphs database (http://molmovdb.org/cgi-bin/search.cgi). We selected a combination (Morph ID: 814007-14919) of Ca^{2+}/CaM/RS20 complex (PDB: 1cdl) and Ca^{2+}/CaM (PDB: 1cll) as two kinds of data sources, because only these two structures are solved by the same group and accordingly the information flow in the Flores' method (*34*) will be processed without ambiguity. Between these two structures, 18 sequential predicted morphs of CaM (from ff0 form (PDB: 1cdl) to ff17 form (PDB: 1cll) were obtained, and three conformations of them (ff11, ff13, and ff15) were selected with reference of experimental data (R_g, distances between their two globular domains, and shapes of Kratky plot) to their calculated ones. After placements of p17 to the three morphs and energy minimizations of the complexes, their parameters have calculated again, and a predicted model (ff15 derivative) of the complex whose calculated parameters agreed with the experimental data well selected as the final 3D model.

Figure 5 shows the stereoview of a tertiary structural model predicted for the candidate, which best fits the SAXS data. The two domains of CaM remain essentially unchanged upon complexation. The hinge motions, however, occur in the central linker region of CaM, in which the electrostatic residues 74, 78, and 82 interact with N-terminal residues of the peptide. The acidic residues in the N-terminal domain interact with basic residues in a central part of the peptide, thereby enabling the central part to change the conformation, while an acidic residue in the C-terminal domain interacts with two basic residues in the two helical sites of the peptide. Figure 6 shows a close-up of the central helix region (residues 66−92) in the ff15 derivative as well as the corresponding regions in the ff0 and ff17 forms. The helix of this region in the ff15 derivative is rather disentangled in comparison with the initial forms, although the structure still holds an almost straight one because of the binding of the peptide. Thus, the central helix region of CaM could play an important role as a hinge in the building up of the 3D

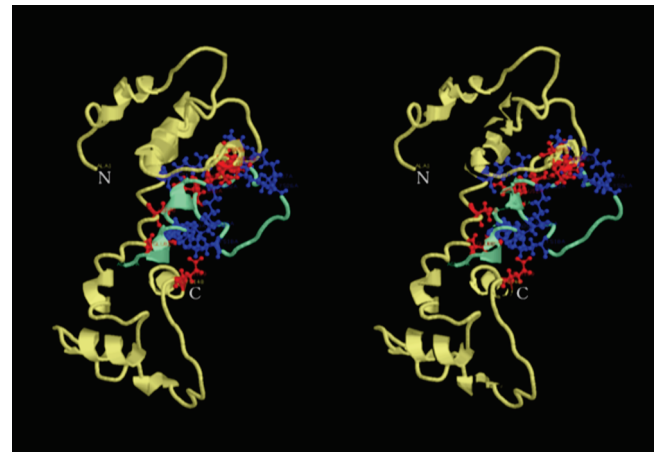

FIGURE 5: Stereoview of a tertiary structural model predicted for the complex of Ca^{2+}/CaM/p17(11−47). The yellow drawing denotes Ca^{2+}/CaM (yellow), and the green drawing denotes p17(11−47). Acidic (red) and basic (blue) residues related to residue pairs inferred purely from the model are shown by ball and stick. The stereoview was obtained using RasWin (version 2.7.3).

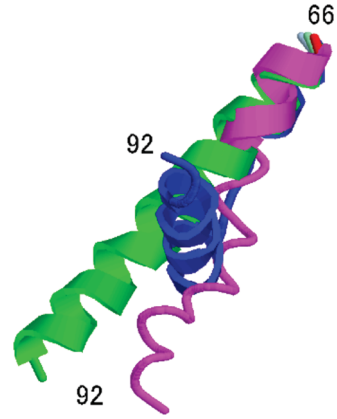

FIGURE 6: Representation of a final structure of the central helix region (residues 66−92) in the ff15 derivative (magenta); the corresponding regions in the ff0 (PDB: 1cll, blue) and ff17 forms (PDB: 1cdl, green) are also shown as a reference.

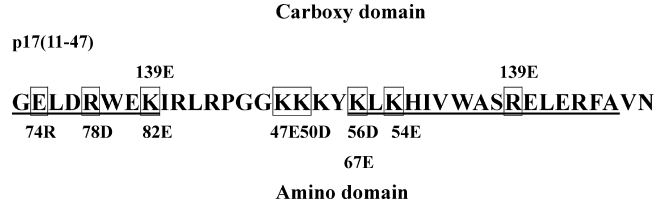

FIGURE 7: Summary of residue pairs inferred purely from the model shown in Figure 5. Residues in p17(11−47) involved in electrostatic interactions are boxed. Underlined sequences denote helices, which were referred from the Protein Data Bank code of p17 (1tam). Carboxy domain and amino domain denote two domains of CaM, respectively. A number with one letter is the amino acid numbering in a CaM sequence.

model of the complex. The overall structure of the complex adopts an extended structure with the radius of gyration of 20.5 Å and the interdomain distance of 34.2 Å. It is noted that the latter value is in good agreement with the corresponding value of 32.7 Å evaluated from DAMMIN. Figure 7 shows a summary of residue pairs inferred purely from the model shown in Figure 5. Ca^{2+}/CaM interacts principally with p17(11−47) via their electrostatic interactions. This result is quite different from that expected in the previous

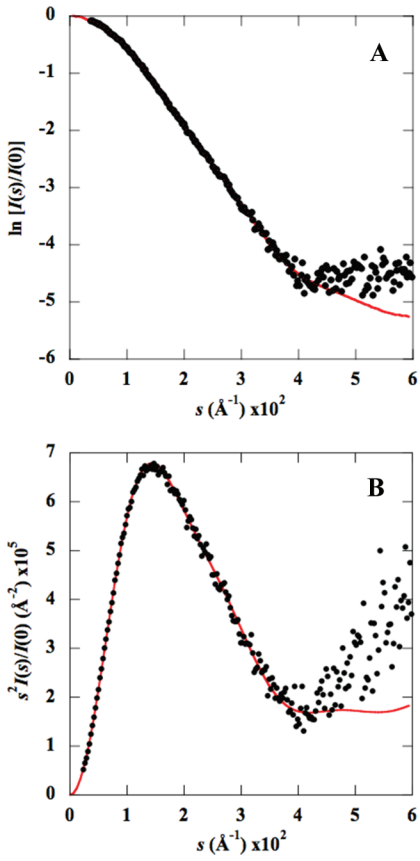

FIGURE 8: Comparison of the experimental scattering data for the Ca^{2+}/CaM/p17(11−47) complex and the calculated curve (red line) for the present model (A). Comparison of the experimental Kratky plot for the Ca^{2+}/CaM/p17(11−47) complex and the calculated curve (red line) for the model (B). According to the description by Piltz (p 239 in ref *32*), the experimental scattering data were extrapolated to zero concentration using a series of concentrations.

section and does not accompany any drastic conformational change of p17.

Figure 8 shows a comparison of the experimental scattering data for the Ca^{2+}/CaM/p17(11−47) complex and the calculated curve for the present model. The experimental value of R_0 is 20.5 ± 0.3 Å, which is in good agreement with the calculated value (20.5 Å) from the coordinates of the model. Thus, the resultant coordinates of the complex obtained from the present model show a reasonable fitting of the SAXS data except the deviation beyond $s = 0.043$ Å^{-1}. Beyond $s = 0.043$ Å^{-1}, the calculated curves deviate from the experimental data, suggesting the limits of the present model prediction. The deviation might be improved by taking correctly into account of the secondary structure, which is highly sensitive to environmental effects (*45, 46*). As the SAXS method is not especially suitable for obtaining information on the secondary structure, other information containing circular dichroism (CD) will be needed to improve the calculated profile beyond $s = 0.043$ Å^{-1}. As such a deviation was observed for both Ca^{2+}/CaM and Ca^{2+}/CaM/skMLCK22 complex, however, this could not be in part an instrumental bias. In addition, it should be noted that the present analysis is free from any adjustable parameter, as the present SAXS profile is normalized.

The present result suggests that the two groups of bulky hydrophobic residues of p17(11−47) are not responsible for the binding with two domains of CaM and that the hydrophobic domains of Ca^{2+}/CaM interact with the myristic acid moiety of p17, if the model mimics the corresponding part of a Ca^{2+}/CaM/p17 complex. The present result also suggests that Ca^{2+}/CaM plays a role in a myristyl switch model of Gag membrane targeting (*47, 48*). To study the interaction of CaM with the whole structure of p17, we used p17(11−47) as the model peptide in this report. This may only imperfectly mimic the interaction of CaM with the whole structure of p17. Further studies will be needed to confirm this point.

ACKNOWLEDGMENT

We thank Prof. Katsumi Kobayashi for help in the SR-SAXS measurements.

REFERENCES

1. Eldik, L. J. V., and Watterson, D. M. (1998) *Calmodulin and Calcium Signal Transduction*, Academic Press, San Diego.
2. Means, A. R., VanBerkum, M. F. A., Baguchi, I., Lu, K. P., and Rasmussen, C. D. (1991) Regulatory functions of calmodulin. *Pharmacol. Ther. 50*, 255–270.
3. Vogel, H. J. (1994) The Merck Frosst Award Lecture 1994. Calmodulin: a versatile calcium mediator protein. *Biochem. Cell. Biol. 72*, 357–376.
4. Seaton, B. A., Head, J. F., Engelman, D. M., and Richards, F. M. (1985) Calcium-induced increases in the radius of gyration and maximum dimension of calmodulin measured by small-angle X-ray scattering. *Biochemistry 24*, 6740–6743.
5. Heidorn, D. B., and Trewhella, J. (1988) Comparison of the crystal and solution structures of calmodulin and troponin C. *Biochemistry 27*, 909–915.
6. Persechini, A., and Kretsinger, R. H. (1988) The central helix of calmodulin functions as a flexible tether. *J. Biol. Chem. 263*, 12715–12178.
7. Barbato, G., Ikura, M., Kay, L. E., Pastor, R. W., and Bax, A. (1992) Backbone dynamics of calmodulin studied by ^{15}N relaxation using inverse detected two-dimensional NMR spectroscopy: the central helix is flexible. *Biochemistry 31*, 5269–5278.
8. Ikura, M., Clore, G. M., Gronenborn, A. M., Zhu, G., Klee, C. G., and Bax, A. (1992) Solution structure of a calmodulin-target peptide complex by multidimensional NMR. *Science 256*, 632–638.
9. Meadow, W. E., Means, A. R., and Quiocho, F. A. (1992) Target enzyme recognition by calmodulin: 2.4 Å structure of a calmodulin-peptide complex. *Science 257*, 1251–1255; (1993) Modulation of calmodulin plasticity in molecular recognition on the basis of X-ray structures, *Science 262*, 1718−1721.
10. Hoeflich, K. P., and Ikura, M. (2002) Calmodulin in action: diversity in target recognition and activation mechanisms. *Cell 108*, 739–742.
11. Radding, W., Williams, J. P., McKenna, M. A., Tummala, R., Hunter, E., Tytler, E. M., and McDonald, J. M. (2000) Calmodulin and HIV type 1: interactions with Gag and Gag products. *AIDS Res. Hum. Retroviruses 16*, 1519–1525.
12. Gelderblom, H. R., Hausmann, E. H., Ozel, M., Pauli, G., and Koch, M. A. (1987) Fine structure of human immunodeficiency virus (HIV) and immunolocalization of structural proteins. *Virology 156*, 171–176.
13. Gelderblom, H. R. (1991) Assembly and morphology of HIV: potential effect of structure on viral function. *AIDS 5*, 617–638.
14. Bryant, M., and Ratner, L. (1990) Myristoylation-dependent replication and assembly of human immunodeficiency virus 1. *Proc. Natl. Acad. Sci. U.S.A. 87*, 523–527.
15. Freed, E. O., Orenstein, J. M., Buckler-White, A. J., and Martin, M. A. (1994) Single amino acid changes in the human immunodeficiency virus type 1 matrix protein block virus particle production. *J. Virol. 68*, 5311–5320.
16. Pal, R., Reitz, M. S., Jr., Tschachler, E., Gallo, R. C., Sarngadharan, M. G., and Veronese, F. D. (1990) Myristoylation of gag proteins of HIV-1 plays an important role in virus assembly. *AIDS Res. Hum. Retroviruses 6*, 721–730.

17. Freed, E. O., Englund, G., and Martin, M. A. (1995) Role of the basic domain of human immunodeficiency virus type 1 matrix in macrophage infection. *J. Virol. 69*, 3949–3954.
18. Yuan, X., Yu, X., Lee, T.-H., and Essex, M. (1993) Mutations in the N-terminal region of human immunodeficiency virus type 1 matrix protein block intracellular transport of the Gag precursor. *J. Virol. 67*, 6387–6394.
19. Zhou, W., Parent, L. J., Wills, J. W., and Resh, M. D. (1994) Identification of a membrane-binding domain within the amino-terminal region of human immunodeficiency virus type 1 Gag protein which interacts with acidic phospholipids. *J. Virol. 68*, 2556–2569.
20. Dorfman, T., Mammano, F., Haseltine, W. A., and Gottlinger, H. G. (1994) Role of the matrix protein in the virion association of the human immunodeficiency virus type 1 envelope glycoprotein. *J. Virol. 68*, 1689–1696.
21. Yu, X., Yuan, X., Matsuda, Z., Lee, T.-H., and Essex, M. (1992) The matrix protein of human immunodeficiency virus type 1 is required for incorporation of viral envelope protein into mature virions. *J. Virol. 66*, 4966–4971.
22. Freed, E. O., and Martin, M. A. (1995) Virion incorporation of envelope glycoproteins with long but not short cytoplasmic tails is blocked by specific, single amino acid substitutions in the human immunodeficiency virus type 1 matrix. *J. Virol. 69*, 1984–1989.
23. Freed, E. O., and Martin, M. A. (1996) Domains of the human immunodeficiency virus type 1 matrix and gp41 cytoplasmic tail required for envelope incorporation into virions. *J. Virol. 70*, 341–351.
24. Ono, A., Huang, M., and Freed, E. O. (1997) Characterization of human immunodeficiency virus type 1 matrix revertants: effects on virus assembly, Gag processing, and *Env* incorporation into virions. *J. Virol. 71*, 4409–4418.
25. Hayashi, N., Matsubara, M., Takasaki, A., Titani, K., and Taniguchi, H. (1998) An expression system of rat calmodulin using T7 phage promoter in *Escherchia coli*. *Protein Expression Purif. 12*, 25–28.
26. Yazawa, M., Sakuma, M., and Yagi, K. (1980) Calmodulins from muscles of marine invertebrates, scallop and sea anemone. *J. Biochem. 87*, 1313–1320.
27. Izumi, Y., Kuwamoto, S., Jinbo, Y., and Yoshino, H. (2001) Increase in the molecular weight and radius of gyration of apocalmodulin induced by binding of target peptide: evidence for complex formation. *FEBS Lett. 495*, 126–130.
28. Lowry, O. H., Rosenbrough, N. J., Farr, A. L., and Randall, R. J. (1951) Protein measurement with the Folin phenol reagent. *J. Biol. Chem. 193*, 265–275.
29. Ueki, T., Hiragi, Y., Kataoka, M., Inoko, Y., Amemiya, Y., Izumi, Y., Tagawa, H., and Muroga, Y. (1985) Aggregation of bovine serum albumin upon cleavage of its disulfide bonds studied by the time-resolved small-angle X-ray scattering technique with synchrotron radiation. *Biophys. Chem. 23*, 115–124.
30. Guinier, A., and Fournet, G. (1955) *Small-Angle Scattering of X-Rays*, John Wiley & Sons, New York.
31. Izumi, Y., Wakita, M., Yoshino, H., and Matsushima, N. (1992) Structure of the proteolytic fragment F34 of calmodulin in the absence and presence of mastoparan as revealed by solution X-ray scattering. *Biochemistry 31*, 12266–12271.
32. Glatter, O., and Kratky, O. (1982) *Small Angle X-ray Scattering*, Academic Press, London.
33. Svergun, D. I. (1992) Determination on the regularization parameter in indirect-transform methods using perceptual criteria. *J. Appl. Crystallogr. 25*, 495–503; (1999) Restoring low resolution structure of biological macromolecules from solution scattering using simulated annealing, *Biophys. J. 76*, 2879−2886.
34. Flores, S., Echols, N., Milburn, D., Hespenheide, B., Keating, K., Lu, J., Wells, S., Yu, E. Z., Thorpe, M., and Gerstein, M. (2006) The database of macromolecular motions: new features added at the decade mark. *Nucleic Acids Res. 34*, D296−D301.
35. Furuhashi, Y., Iwata, T., Sikorski, P., Atkins, E., and Doi, Y. (2000) Structure and morphology of the aliphatic polyester poly-β-propiolactone in solution-grown chain-folded lamellar crystals. *Macromolecules 33*, 9423–9431.
36. Hubbard, S. R., Hodgson, K. O., and Doniach, S. (1988) Small-angle X-ray scattering investigation of the solution structure of troponin C. *J. Biol. Chem. 263*, 4151–4158; Hubbard, S. R. (1987) Small-angle X-ray scattering studies of calcium-binding proteins, Ph.D. Thesis, Stanford University, Stanford, CA.
37. Yokouchi, T., Nogami, H., Izumi, Y., Yoshino, H., Nakashima, K. I., and Yazawa, M. (2003) Solution X-ray scattering data show structural differences among chimeras of yeast and chicken calmodulin: Implications for structure and function. *Biochemistry 42*, 2195–2201.
38. Matsushima, N., Izumi, Y., Matsuo, T., Yoshino, H., Ueki, T., and Miyake, Y. (1989) Binding of both Ca^{2+} and mastoparan to calmodulin induces a large change in the tertiary structure. *J. Biochem. 105*, 883–887.
39. Heidorn, D. B., Seeger, P. A., Rokop, S. E., Blumenthal, D. K., Means, A. R., Crespi, H., and Trewhella, J. (1989) Changes in the structure of calmodulin induced by a peptide based on the calmodulin-binding domain of myosin light chain kinase. *Biochemistry 28*, 6757–6764.
40. Kataoka, M., Head, J. F., Seaton, B. A., and Engelman, D. M. (1989) Melittin binding causes a large calcium-dependent conformational change in calmodulin. *Proc. Natl. Acad. Sci. U.S.A. 86*, 6944–6948.
41. Izumi, Y., Amano, A., Saito, T., and Jinbo, Y. (2007) Solution structure of Ca^{2+}/calmodulin complexed with a lentivirus lytic peptide 1 reveals a novel mode of molecular recognition. *J. Appl. Crystallogr. 40*, S170−S174.
42. Yoshino, H., Minari, O., Matsushima, N., Ueki, T., Miyake, Y., Matsuo, T., and Izumi, Y. (1989) Calcium-induced shape change of calmodulin with mastoparan studied by solution X-ray scattering. *J. Biol. Chem. 264*, 19706–19709.
43. Massiah, M. A., Starich, M. R., Paschall, C., Summers, M. F., Christensen, A. M., and Sundquist, W. I. (1994) Three-dimensional structures of the human immunodeficiency virus type 1 matrix protein. *J. Mol. Biol. 244*, 198–223.
44. Matthews, S., Barlovo, P., Clark, N., Kingsman, S., Kingsman, A., and Campbell, I. (1995) Refined solution structure of p17, the HIV matrix protein. *Biochem. Soc. Trans. 23*, 725–729.
45. Bayley, P., Martin, S., and Jones, G. (1988) The conformation of calmodulin: a substantial environmentally sensitive helical transition in Ca_4-calmodulin with potential mechanistic function. *FEBS Lett. 238*, 61–66.
46. Bayley, P. M., and Martin, S. R. (1992) The α-helical content of calmodulin is increased by solution conditions favoring protein crystallization. *Biochim. Biophys. Acta 1160*, 16–21.
47. Hermida-Matsumoto, L., and Resh, M. D. (1999) Human immunodeficiency virus type 1 protease triggers a myristoyl switch that modulates membrane binding of Pr55 gag and p17MA. *J. Virol. 73*, 1902–1908.
48. Paillart, J. C., and Gottlinger, H. G. (1999) Opposing effects of human immunodeficiency virus type 1 matrix mutations support a myristyl switch model of gag membrane targeting. *J. Virol. 73*, 2604–2612.

BI702416B